Available online at www.sciencedirect.com
ScienceDirect
Earth and Planetary Science Letters 252 (2006) 467–480
EPSL
www.elsevier.com/locate/epsl

The 1994–2004 Al Hoceima (Morocco) earthquake sequence: Conjugate fault ruptures deduced from InSAR

Ahmet M. Akoglu [a,*], Ziyadin Cakir [b,c], Mustapha Meghraoui [b], Samir Belabbes [b], Sidi O. El Alami [d], Semih Ergintav [e], H. Serdar Akyüz [c]

[a] *Eurasian Institute of Earth Sciences, ITU, Istanbul, Turkey*
[b] *EOST-Institut de Physique du Globe, UMR 7516 CNRS, Strasbourg, France*
[c] *Department of Geological Engineering, ITU, Istanbul, Turkey*
[d] *Laboratoire de Geophysique, CNRST, Rabat, Morocco*
[e] *TUBITAK Marmara Research Center, Earth and Marine Sciences Inst., Gebze-Kocaeli, Turkey*

Received 30 March 2006; received in revised form 3 October 2006; accepted 3 October 2006
Available online 14 November 2006
Editor: C.P. Jaupart

Abstract

We study the May 26, 1994 (Mw=6.0) and February 24, 2004 (Mw=6.4) earthquakes that affected the Al Hoceima region of northern Morocco. These events are the two strongest earthquakes recorded in this region. Yet, the exact location, kinematics and relationships between these earthquakes are poorly known since neither of them produced surface ruptures. Using Synthetic Aperture Radar interferometry (InSAR) we mapped the surface displacement field of the two earthquakes to characterize their seismic source parameters. Analysis of the interferograms constructed from ascending and descending orbits for both earthquakes and subsequent elastic modeling using slip inversions on triangular fault patches suggest that the two mainshocks occurred on blind conjugate strike–slip faults; the 1994 earthquake being associated with N23° E trending left-lateral fault and the 2004 earthquake with N45° W trending right-lateral fault. This result contradicts previous inferences on the kinematics, location and rupture geometry of the earthquakes deduced from conventional analyses of seismic waveforms and aftershocks distribution. The InSAR analysis reveals the fragmentation of the Rif Mountain throughout a complex network of conjugate blind faults consistent with the transpression tectonics along the plate boundary in North Africa. Although the two earthquakes took place in the Rif thrust-and-fold belt, the late Quaternary deformation indicates E–W extension in agreement with the NW–SE and NE–SW trending conjugate strike–slip faulting.

Keywords: InSAR; Al Hoceima; Conjugate faulting; Rif; Morocco

1. Introduction

The city of Al Hoceima and Rif Mountains, located on the Mediterranean coast in northern Morocco (Fig. 1), was struck by two strong earthquakes within 10 yr; first on May 26, 1994 (Mw=6.0) and later on February 24, 2004 (Mw=6.4) (Fig. 2). The latter produced severe damage (about 600 deaths and more than 2500 buildings destroyed) in Al Hoceima and the surrounding areas [1]. These two events are the strongest earthquakes in the period of instrumental seismicity to strike the eastern part of the Rif Mountain range, a thrust-and-fold belt within the east–west trending Africa–Eurasia plate boundary in

* Corresponding author. Fax: +90 212 285 6210.
E-mail address: Ahmet.Akoglu@itu.edu.tr (A.M. Akoglu).

0012-821X/$ - see front matter © 2006 Elsevier B.V. All rights reserved.
doi:10.1016/j.epsl.2006.10.010

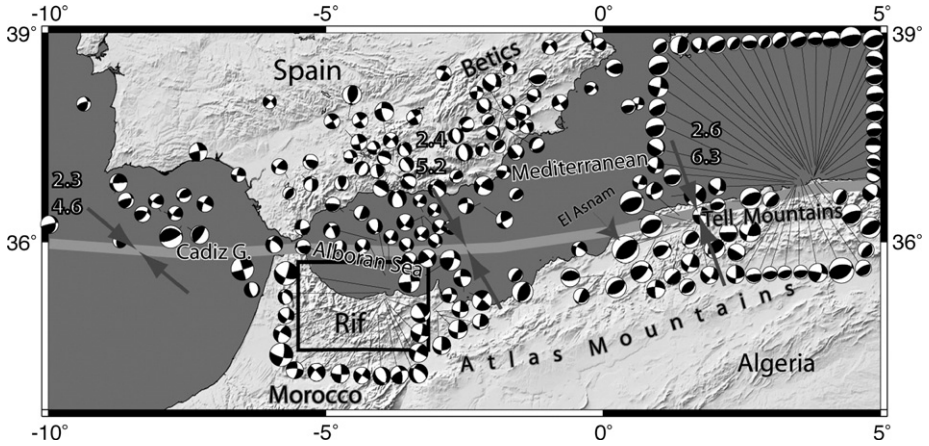

Fig. 1. Shaded relief map of eastern Mediterranean with focal mechanism solutions of earthquakes between 1951 and 2005 (data from Buforn et al. [14], Instituto Geografico Nacional and Swiss Seismological Service). Note the change in the type of deformation from Algeria in the east to Gulf of Cadiz in the west along the African–Eurasian plate boundary (thick gray line with arrows illustrating the direction of convergence in mm/yr) [2,12]. Black rectangle shows the location of Fig. 2 in eastern Rif.

the western Mediterranean [2] (Fig. 1). The epicenters of the earthquakes are reported to be close to each other and located 15–20 km south west of Al Hoceima (Fig. 2). However, the source parameters of these earthquakes are not known in detail because (1) neither of them produced surface ruptures (i.e. both took place on blind faults) [1,3,4]; (2) the absence of obvious morphological features typical of active faults prevents a clear identification of the causative seismogenic faults in the epicentral region; (3) the regional network is too sparse to monitor and precisely locate the seismic activity [4]; and (4) aftershocks collected by local networks are complex and distributed [3,5,6].

Focal mechanism solutions indicate that the two earthquakes are associated with oblique strike–slip faults trending either NE–SW with left-lateral slip or NW–SE with right-lateral slip (Table 1). Despite the disagreements in the location and geometry of the coseismic fault

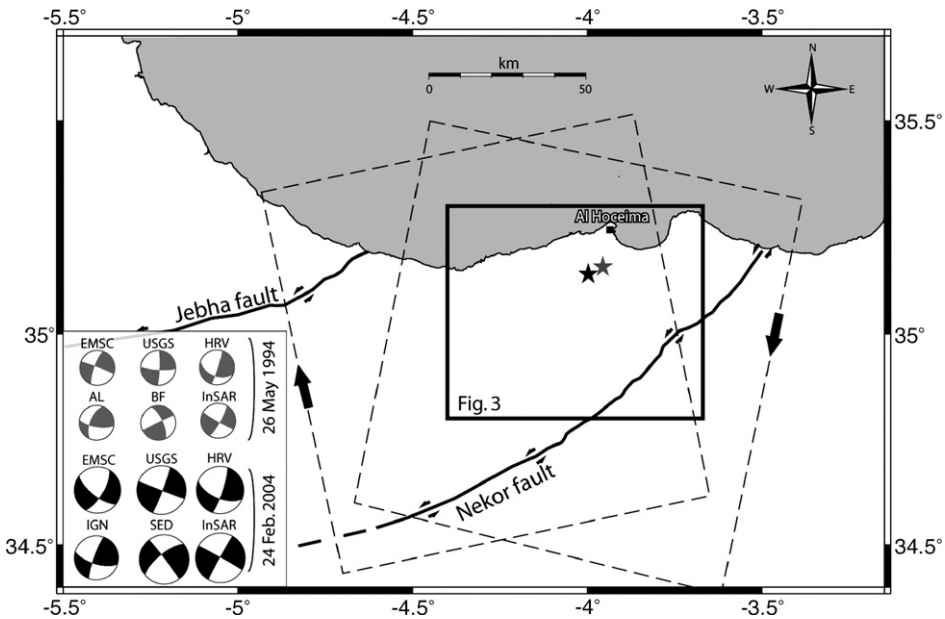

Fig. 2. Map of the study area showing the ERS/ENVISAT radar frames (dashed rectangles with arrows indicating the satellite flight direction) for ascending and descending orbits. Heavy black lines are major strike–slip faults in the region. Beachballs are focal mechanism solutions of the May 26, 1994 and February 24, 2004 Al Hoceima earthquakes from various sources (gray and black solutions, respectively). The epicenters indicated by stars are from Calvert et al. [5] and USGS. Black box shows the location of Figs. 3, 4, 7 and 8.

Table 1
Focal mechanism solutions of the 26 May 1994 and 24 February 2004 Al Hoceima earthquakes

	Source	Lon.	Lat.	Depth (km)	Mo (N.m) 10^{18}	Mw	Plane 1			Plane 2		
							Strike	Dip	Rake	Strike	Dip	Rake
2004	SED	−3.997	35.142	12.0	5.18	6.4	115	84	157	208	67	7
	HRV	−3.840	35.270	12.0	3.93	6.3	113	61	−170	18	81	−29
	IGN	−3.997	35.142	6.0	2.70	6.2	107	67	171	200	82	23
	IAG	−4.000	35.140	–	2.88	6.3	107	73	−161	11	72	−17
	USGS	−3.997	35.142	13.0	4.90	6.4	111	89	−176	21	86	−1
	EMSC	−4.000	35.000	29.0	3.60	6.3	128	69	−158	30	69	−23
	InSAR	−3.993	35.127	6–10	6.60	6.5	322	87	−161	231	71	−3
1994	BB	−3.920	35.160	7	1.18	6.0	335	69	2	244	88	178
	USGS	−4.100	35.305	9	0.97	6.0	93	80	−174	2	84	−6
	HRV	3.910	35.370	10	1.01	5.9	112	48	−173	17	85	−7
	AL	3.990	35.280	13	–	–	100	70	157	202	60	23
	EMSC	−4.100	35.305	–	–	–	291	86	−166	200	76	−14
	InSAR	−4.039	35.202	6–10	2.00	6.1	292	84	−170	23	80	−6

SED: Swiss Seismological Service, HRV: Harvard, IGN: Instituto Geografico Nacional, IAG: Instituto Andaluz de Geofisica, USGS: United States Geological Survey, EMSC: European–Mediterranean Seismological Centre, BB: Bezzeghoud and Buforn [7], AL: El Alami et al. [3]. InSAR: this study.

ruptures, seismic studies based on aftershock distribution, wave modeling and apparent source time functions imply that the two earthquakes have left-lateral mechanisms [3,5–9]. In contrast to the seismic observations, the recent analysis and modeling of Envisat InSAR data provided by Cakir et al. [10] suggest that the 2004 earthquake took place most likely on a NW–SE trending right-lateral fault. In this previous work, Cakir et al. [10] indicated how the left-lateral solutions for the 2004 earthquake conflict with the InSAR data, whereas the likely model with right-lateral faulting was illustrated and discussed in detail.

In this paper, we study the two earthquakes of 1994 and 2004, and their relationship using ERS and Envisat SAR data. We model the interferograms of the two earthquakes with a particular attention to the 1994 event using dislocations on triangular faults embedded in a homogenous and elastic half space [11]. The availability of ascending and descending interferograms for both earthquakes allows us to constrain their rupture parameters with high confidence. The existence of conjugate faults shed light on the understanding of regional tectonics and related seismic hazard assessment in this region. Finally, we discuss the kinematics of conjugate faults and implications of coseismic strike–slip ruptures within the Africa–Eurasia plate boundary deformation zone.

2. Seismotectonic setting

The Rif Cordillera belong to the E–W trending thrust-and-fold system of north Africa that results from the collision between Africa and Eurasia. The system includes the Tell Atlas mountain ranges of Algeria and Tunisia along the Mediterranean coast to the east, and forms a collision tectonics strip along the African–Eurasian plate boundary. Based on the global plate models and GPS observations, the rate of the ongoing shortening between Africa and Eurasia decreases towards the west from 6.3 to 2.3 mm/yr from Sicily to northern Morocco (Fig. 1) [12]. The pattern of active deformation can be interpreted as an anticlockwise rotation of Africa relative to Eurasia with an approximate Euler pole location between 2.1 and 21.0 in latitude and −20.0 and −18.3 in longitude [2,13]. Despite the apparent coherent plate rotation in a global scale, the seismicity along the plate boundary is rather complex and varies significantly from west to east [14]. The recent seismicity and the 1994–2004 Al Hoceima seismic sequence indicate that the Rif is being deformed under a strike–slip tectonic regime. However, adjacent regions in northern Algeria to the east and the Gulf of Cadiz to the west, are subject to thrust faulting deformation [15,16]. Further seismological observations over longer timescales are required to determine if the rate of seismicity along the plate boundary reflects the change in the shortening rate from east to west.

Neotectonic features of the Rif consist of the major Nekor and Jebha, left-lateral strike–slip faults of NE–SW trend (Fig. 2), accompanied by north–south trending normal faults that form a graben-like structure east of Al Hoceima city and a conjugate network of relatively small (10 to 20-km-long) NW–SE and NE–SW strike–slip faults (Fig. 3). The transpressive tectonics and existence of a complex fault network with thrust, normal and strike–slip faulting in the Rif probably reflect the rapidly changing local tectonic regime with block rotations

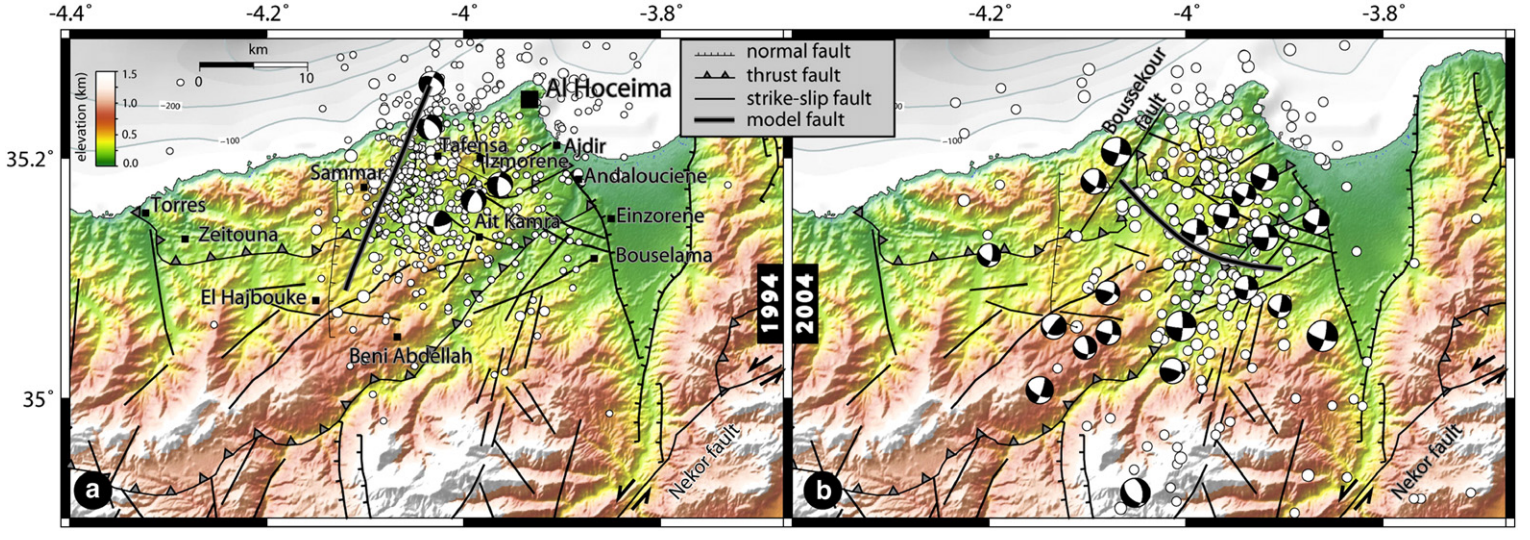

Fig. 3. Morphotectonic framework of the Al Hoceima region with aftershocks distribution of the 1994 (a) and 2004 (b) earthquakes from El Alami et al. [3] and IGN (compiled from Calvert et al. [5], El Alami et al. [3], and Ait-Brahim et al. [43]).

during the Neogene and Quaternary [17]. Although the region exhibited fairly moderate seismicity in the instrumental period before the 1994 earthquake, several strong earthquakes are known to have occurred in the historical times, the largest one being the 1801 event [4,18]. However, further work in the Rif region is required to identify the active and seismogenic faults that can be associated with such large historical seismic events. Microseismic observations suggest that the Nekor fault that once acted as a major continental strike–slip fault until late Miocene [19], is now probably inactive due to the changes in the regional stress field [20].

Although the mechanism of the 1994 earthquake rupture, based on different observations (i.e. aftershock distribution, macroseismicity, regional tectonics and offshore seismic profiles) made by various investigators, is in agreement with left-lateral faulting, there are inconsistencies in the literature regarding the location and geometry of the rupture. While Calvert et al. [5] infer that the rupture lies between Beni Abdellah and Al Hoceima, El Alami et al. [3] propose a fault of similar trend (N20°–30° E) but shifted to about 6–7 km westward (Fig. 3). On the contrary, Bezzeghoud and Buforn [7] infer a complex rupturing with two sub-events on N5° W and N30° W trending faults in the same region. Similar inconsistencies also exist for the 2004 event: while based on apparent source time functions and seismic wave modeling, Stich et al [9] and Buforn et al. [8] deduce NNE–SSW trending left-lateral ruptures south of Al Hoceima, Dorbath et al. [6] based on aftershock distribution infer two possible fault ruptures striking NW–SE with right-lateral or/and NE–SW with left-lateral mechanism. The absence of coseismic surface ruptures and the complex tectonic context clearly require adapted methods of investigations to characterize blind or hidden faults.

3. Analysis of InSAR data

The methodology of Synthetic Aperture Radar Interferometry (InSAR) flourished in the last 15 yrs since its introduction as a tool to investigate earth movements mainly after the Landers earthquake [21,22]. Interferograms calculated by subtracting phase information of radar images before and after an earthquake provide unrivalled high density surface deformation maps with sub-centimeter accuracy. In addition, the technique also allows measurements of subtle earth deformation like postseismic relaxation or interseismic creep [23–25].

In order to examine and model the ground deformation associated with the 1994 and 2004 Al Hoceima earthquakes we used European Space Agency's (ESA) ERS and Envisat SAR data, respectively. While the ERS Level-0 (raw) SAR data were processed using the JPL ROI_PAC software [26], the Envisat Level-1 (single-look) ASAR data were processed using DORIS SAR processing software [27] with 5 azimuth 1 range looks (i.e. averaged to 20×20 m of ground pixel size), and precise satellite orbits from Delft University [28]. The effect of topography which depends on the perpendicular separation between orbital trajectories is removed from the interferograms using the SRTM 3-arc-second ($\sim$90 m) posting digital elevation model [29]. The interferograms were filtered using a weighted power spectrum technique [30]. We obtained a minimum of two coseismic interferograms for each earthquake, one in the ascending and one in the descending imaging geometry of the ERS and Envisat satellites (Table 2). Some of the calculated interferograms are shown in Fig. 4 with wrapped fringes, each representing half a wavelength (i.e. 2.83 cm) range change along the radar line sight. Despite signal decorrelation in the vegetated and cultivated areas away from the coast and in the mountainous

Table 2
SAR data used in this study

	Orbit	Orbit-1	Date-1	Orbit-2	Date-2	Δ Date	$B_\perp$	H_a
1994	**Asc.**	**12399**	**1993-11-28**	**3090**	**1995-11-22**	**724**	**47**	**213**
		12399	**1993-11-28**	**7599**	**1996-10-02**	**1039**	**28**	**359**
		12399	1993-11-28	22763	1995-11-21	723	174	57
	Des.	**11447**	**1993-09-23**	**23314**	**1995-12-30**	**828**	**80**	**125**
		10445	**1993-07-15**	**3140**	**1995-11-26**	**864**	**96**	**104**
2004	**Asc.**	**9302**	**2003-12-10**	**12308**	**2004-07-07**	**210**	**13**	**773**
		9302	2003-12-10	12809	2004-08-11	245	153	65
	Des.	5845	2003-04-13	11857	2004-06-06	420	26	386
		5845	**2003-04-13**	**13360**	**2004-09-19**	**525**	**194**	**51**
		7849	2003-08-31	11857	2004-06-06	280	290	34
		6847	2003-06-22	12358	2004-07-11	385	284	35

Interferometric pairs with bold faces are those shown in Fig. 4. $B_\perp$ perpendicular baseline (m) H_a altitude of ambiguity (i.e. elevation change in meters required to create one fringe due to topography).

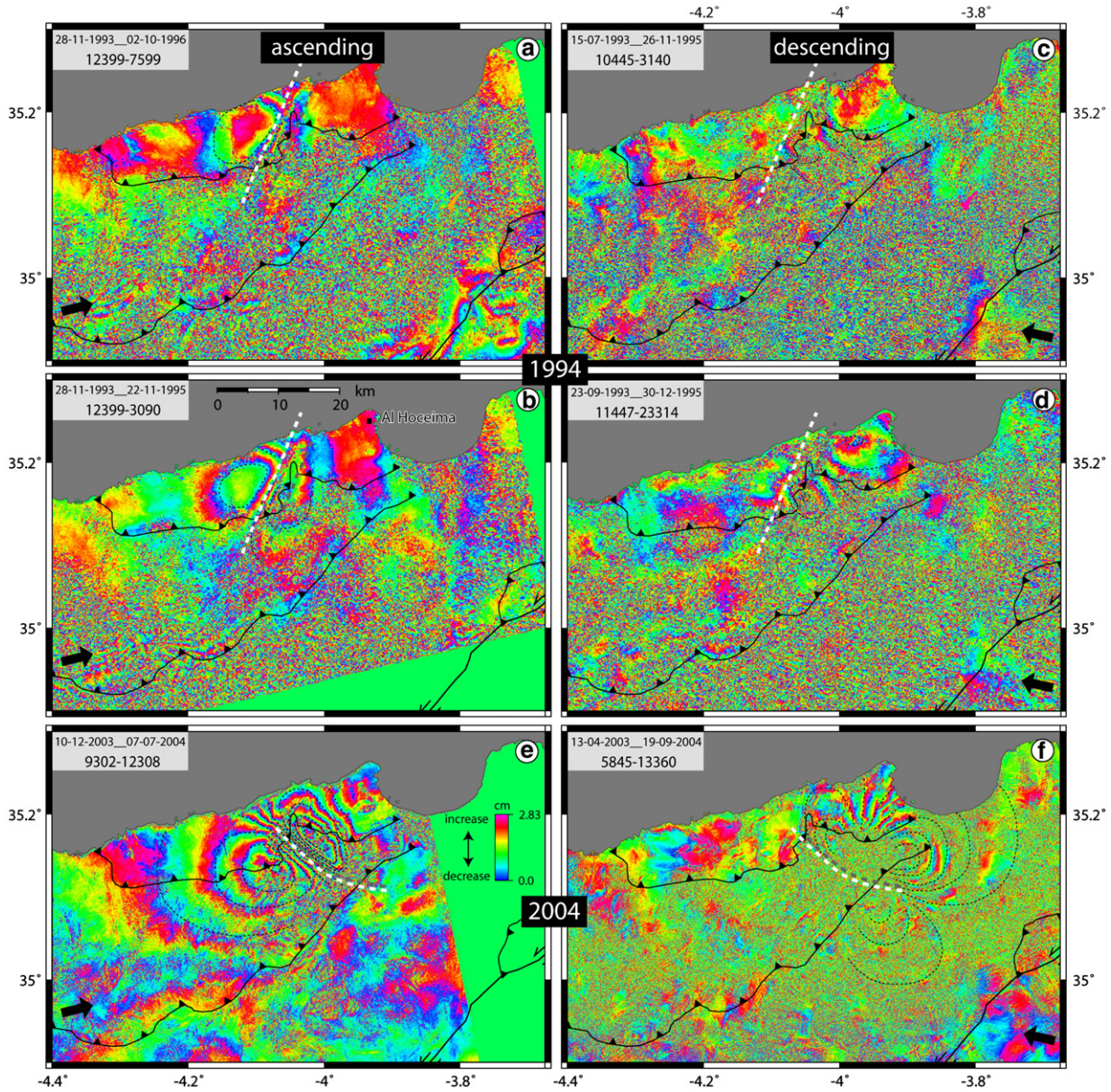

Fig. 4. Coseismic interferograms of the 1994 (a, b, c, d) and 2004 (e, f) earthquakes in the ascending (a, b, e) and descending (c, d, f) radar geometry with arrows indicating the satellite look direction. Each fringe shows 2.83 cm surface deformation along the radar line of sight. Bold white and gray dashed lines are the surface trace of the modeled fault and the surface projection of the bottom line of the modeled fault (at 16.5 km of depth), respectively. Digitized fringe curves are used to invert the coseismic slip on the modeled fault surfaces. Thrust faults are shown for spatial comparison of fringe patterns in the interferograms.

region to south, the interferograms reveal quite well the coseismic deformation fields of the earthquakes in the coastal region of Al Hoceima. Part of the 1994 earthquake however appears to be offshore (Fig. 4). The number of fringes in the interferograms is naturally proportional to the earthquake size with a maximum peak-to-peak line-of-sight (LOS) displacement of about 11 cm (4 fringes) in the 1994 descending interferogram (Fig. 4c,d) and 23 cm (8 fringes) in the 2004 ascending interferogram (Fig. 4e). The low coherence in the earthquake area particularly in the 1994 interferograms is likely due to the changes in the reflective properties of the ground during the long-time span (up to 3 yr) of the interferometric pairs. Having the shortest temporal baseline (7 months), the 2004 ascending interferogram experienced minimum decorrelation.

Table 3
Modeling results with varying fault kinematics and geometry

Model		Length (km)	Depth (km)	Strike (°)	Dip (°)	RMS (cm)			M_o (N m)×10^{18}	Mw
						Ascending	Descending	Average		
Right lateral	1	23	16.5	127	90—	1.37	1.14	1.25	2.0	6.1
	2	23	16.5	122	90—	1.26	0.96	1.11	1.8	6.1
	3	23	16.5	117	90—	1.26	1.13	1.23	1.6	6.0
	4	23	16.5	122	80 NE	1.37	1.45	1.41	1.9	6.1
	5	23	16.5	122	85 NE	1.30	1.17	1.24	1.9	6.1
	6	23	16.5	122	85 SW	1.17	1.00	1.09	1.7	6.1
	7	23	16.5	122	80 SW	1.13	1.06	1.10	1.7	6.1
	8	**23**	16.5	**122**	**75 SW**	**0.82**	**1.23**	**1.03**	**1.3**	**6.0**
	9	23	16.5	122	70 SW	1.04	1.32	1.18	1.4	6.0
Left lateral	10	16	16.5	020	90—	0.86	0.96	0.91	2.1	6.1
	11	16	16.5	023	90—	0.84	0.94	0.89	2.1	6.1
	12	16	16.5	026	90—	0.85	0.94	0.89	2.1	6.1
	13	16	16.5	023	85 SE	0.67	0.79	0.73	2.1	6.1
	14	16	16.5	023	80 SE	0.55	0.72	0.64	2.0	6.1
	15	**16**	16.5	**023**	**77 SE**	**0.53**	**0.70**	**0.62**	**2.0**	**6.1**
	16	16	16.5	023	75 SE	0.54	0.69	0.62	2.0	6.1
	17	16	16.5	023	70 SE	0.65	0.72	0.69	2.0	6.1

Lines with bold faces indicate the best solutions with a right-lateral fault (Model 8) and a left-lateral fault (Model 15).

Availability of independent interferograms in the descending geometry for both earthquakes allows us to confirm that the overall fringe pattern is the same and thus they do not contain any significant atmospheric signal that could potentially be interpreted and hence modeled as surface deformation. The ascending interferograms of each earthquake however share the same pre-earthquake image (Table 2) and thus the possibility of atmospheric artifacts in the ascending interferograms cannot be excluded. The fact that the fringes in the 2004 ascending interferogram are smooth and homogeneous suggests that atmospheric artifacts in the earthquake area are absent or negligible. On the contrary, some of the fringes in the 1994 ascending interferograms are discontinuous and clearly disturbed by atmospheric noise. However, the pattern and distribution of the fringes suggest that they are associated most likely with surface deformation rather than atmospheric signal delay. Analysis of the fringes of 1994 earthquake together with the digital elevation model indicates that there is not any significant correlation between the fringes interpreted as surface deformation and topographic elevation, except the northwestern lobe of the ascending interferogram which may partially contain atmospheric phase. Although atmospheric signal correlated with topography should be negligible in the coastal region, it can be significant to the southwest of the earthquake area where high mountains with considerable elevation changes are present in the topography (Fig. 3). Indeed, the first fringe along the southern thrust fault in the ascending interferogram of the 2004 earthquake is clearly correlated with topography (Fig. 4).

Unlike the Global Positioning System (GPS) that records three components of the coseismic displacement at a benchmark, InSAR records only the component along the line of sight between the satellite and ground point. The line of sight between the point on the ground and the radar satellite in space defines the unit vector. In an East, North, Up coordinate system, the unit vector is

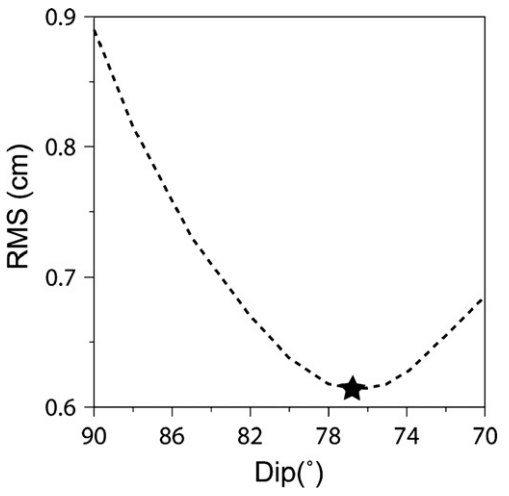

Fig. 5. RMS misfits plot for the southward dip of the rupture plane for distributed-slip models inverted from InSAR data (both ascending and descending). All the other fault parameters are fixed. Star indicates the best-fit dip which is 77° SE.

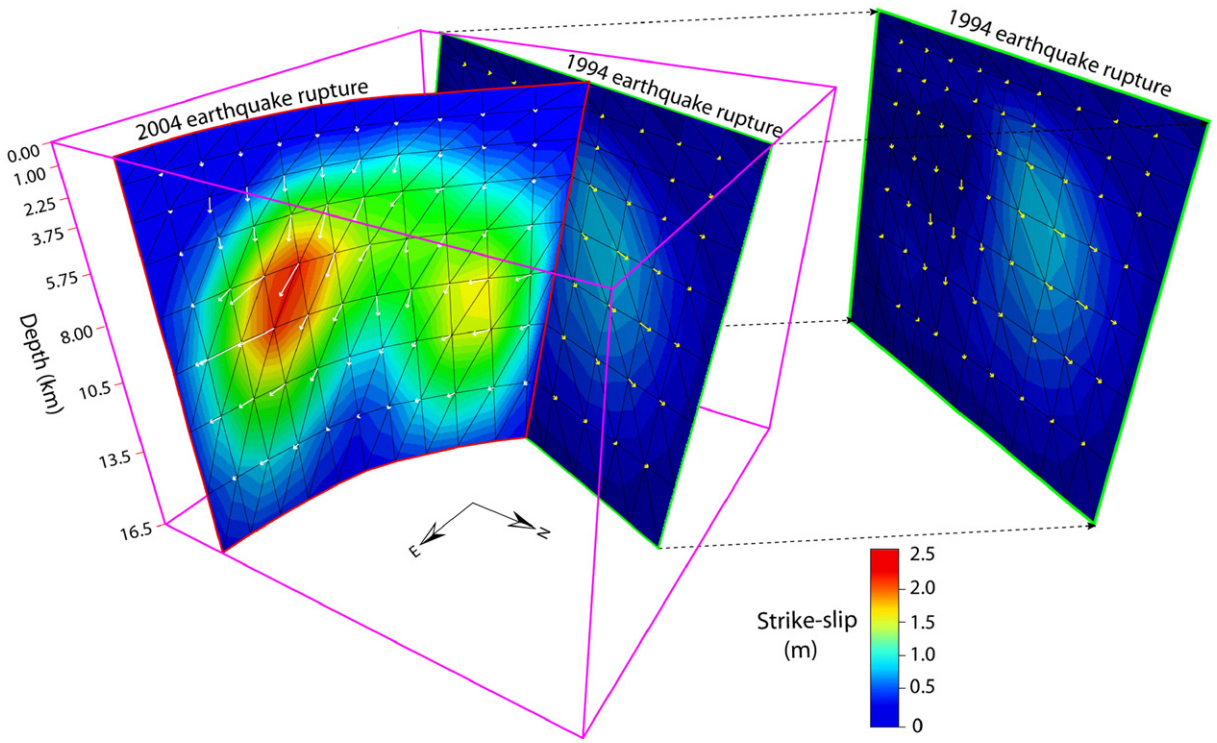

Fig. 6. 3D view of the best slip models of the 1994 and 2004 earthquakes. Strike and dip components of the coseismic slip on each triangular element are inverted using Poly3Dinv (view towards NW). Color maps of the fault surfaces show interpolated strike–slip distribution with arrows indicating the direction of motion of the eastern block relative to the western one. The intersection between the two fault planes may well be the locus of the 2004 earthquake rupture initiation.

+0.39, −0.08, +0.92 for the descending interferogram and −0.41 −0.09, +0.91 for the ascending interferogram, respectively, indicating that the radar is most sensitive to vertical displacements and less sensitive to north–south displacements. Displacements in east–west direction will induce LOS displacement with opposite signs (i.e. range increase or decrease depending on the sense of motion) in descending and ascending interferograms. Consequently, the ascending and descending interferograms of the same earthquake will differ from each other. The difference becomes noteworthy in our case since the surface deformations are related to horizontal displacements on strike–slip faults trending NE–SW or NW–SE at a high angle to the LOS. In some other cases, the overall fringe pattern will remain the same when the fault slip is dominantly vertical (e.g. dip-slip faulting, see Amelung and Bell [31], Talebian et al. [32]), or the pattern will be asymmetric about a *N–S* axis when the faulting mechanism is mainly horizontal in N–S direction [33]. In Fig. 4, the common lobes between the ascending and descending interferograms with the same sense indicate areas where the ground deformation is mainly vertical (i.e. subsidence or uplift depending on the increase or decrease in range change).

Looking at the shape and distribution of the fringe lobes in the coseismic interferograms of the same type (i.e. ascending or descending) one can immediately infer that the two earthquakes must have taken place on two separate faults of different strike since a rotation of roughly 90° is required to match the orientation of the lobes (Fig. 4). This implies that the two earthquakes cannot share a common fault mechanism. From the semicircular shape and distribution of the fringe lobes, it is clear that the 1994 earthquake rupture trends NE–SW in between the two lobes of the ascending interferograms and thus is associated with left-lateral faulting, in agreement with the seismic observations [3,5,7] (Fig. 4a). This in turn implies, in contrast with seismic interpretations of Buforn et al. [8] and Stich et al. [9], that the 2004 event is indeed associated with a right-lateral fault trending NW–SE as suggested by Cakir et al. [10] (Fig. 4e–f). The pattern of fringe lobes and related coseismic displacement fields imply that the two earthquakes took place on blind conjugated strike–slip faults. Indeed, the continuity of fringes across the faults and the location of lobe centers (i.e. zones of maximum deformation) being several kilometers away from the faults, indicate that the 1994 and 2004 coseismic ruptures

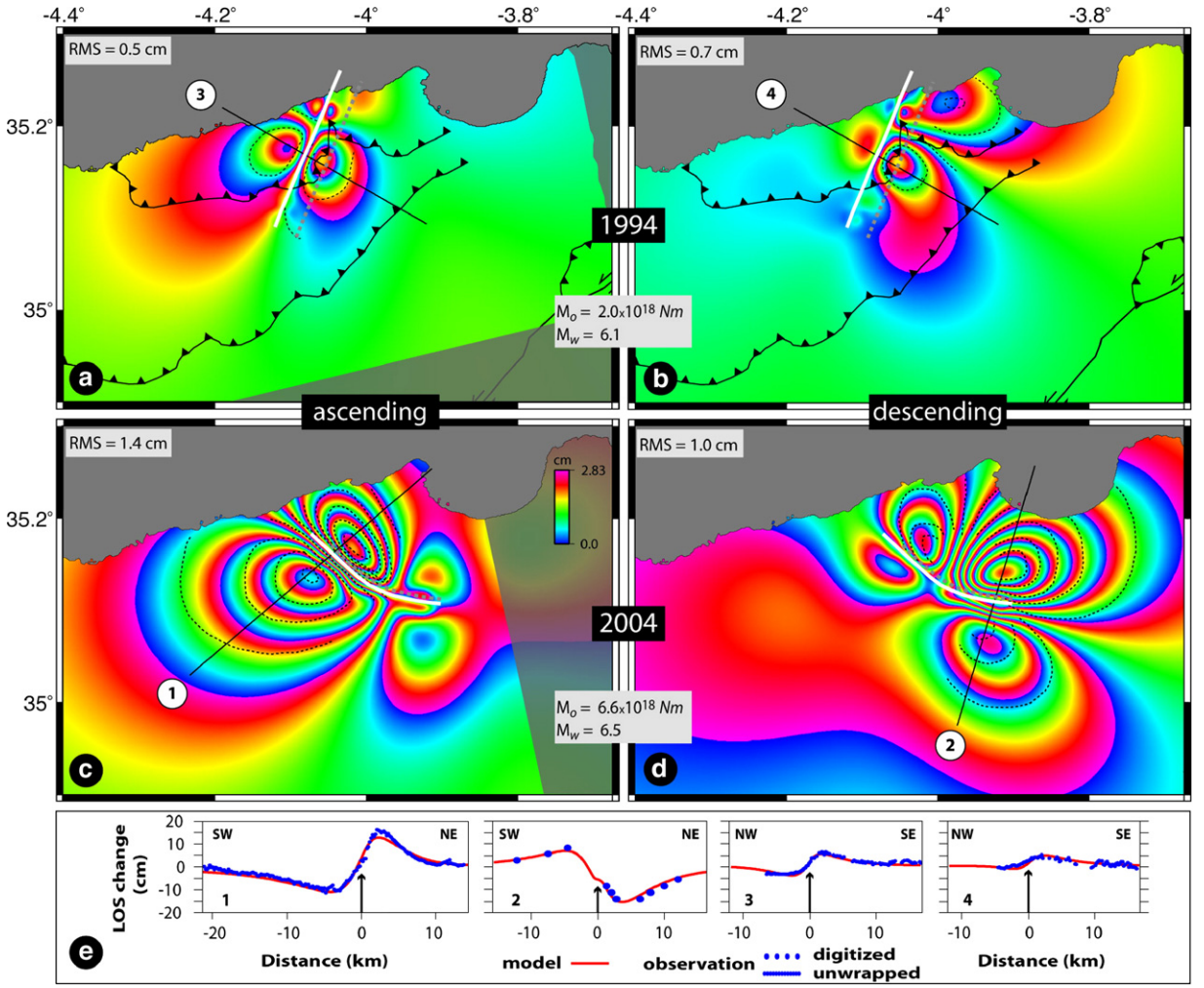

Fig. 7. Modeled interferograms of 1994 (a, b) and 2004 (c, d) earthquakes obtained from inversion of the observed data (fringe lines). Geodetic moment (Mo) and corresponding moment magnitude (Mw) of each earthquake are consistent with those determined from seismology (Table 1). The fit between the data and models is illustrated by line of sight profiles (e). RMS (root mean square) values are in cm.

did not reach the surface and that the significant slip occurred at depth on blind faults rather than at the surface.

4. Elastic modeling of the 1994 and 2004 fault ruptures

The analysis of coseismic interferograms provides significant information on the main characteristics and location of the 1994 and 2004 earthquake ruptures. However, to determine the detailed geometry of fault ruptures and related slip distribution we modeled the interferograms using Poly3Dinv, a 3D-boundary element method that uses triangular dislocations in a linear elastic and homogeneous half-space with a damped least square minimization [34]. As shown below, InSAR data require intersection of the two fault ruptures with the 2004 earthquake fault having a non-planar surface. Therefore, we were able to reconstruct realistic 3D fault surfaces with triangular elements using Poly3D [35], avoiding gaps and overlaps that are otherwise inevitably encountered when modeling curved or segmented faults with rectangular dislocations. This method improves the fit to the geodetic data particularly in the near field when modeling complicated fault ruptures [34,36].

Fault surfaces meshed with triangles were constructed using MATLAB®. While the length of the triangular elements is kept approximately the same (1.7–2 km) along the fault, their sizes are gradually increased from 1 km to 3.5 km along the dip direction down to 16.5 km of depth because the resolution of inverted slip decreases with increasing depth. Instead of unwrapped data, digitized fringes are used in the inversion because most

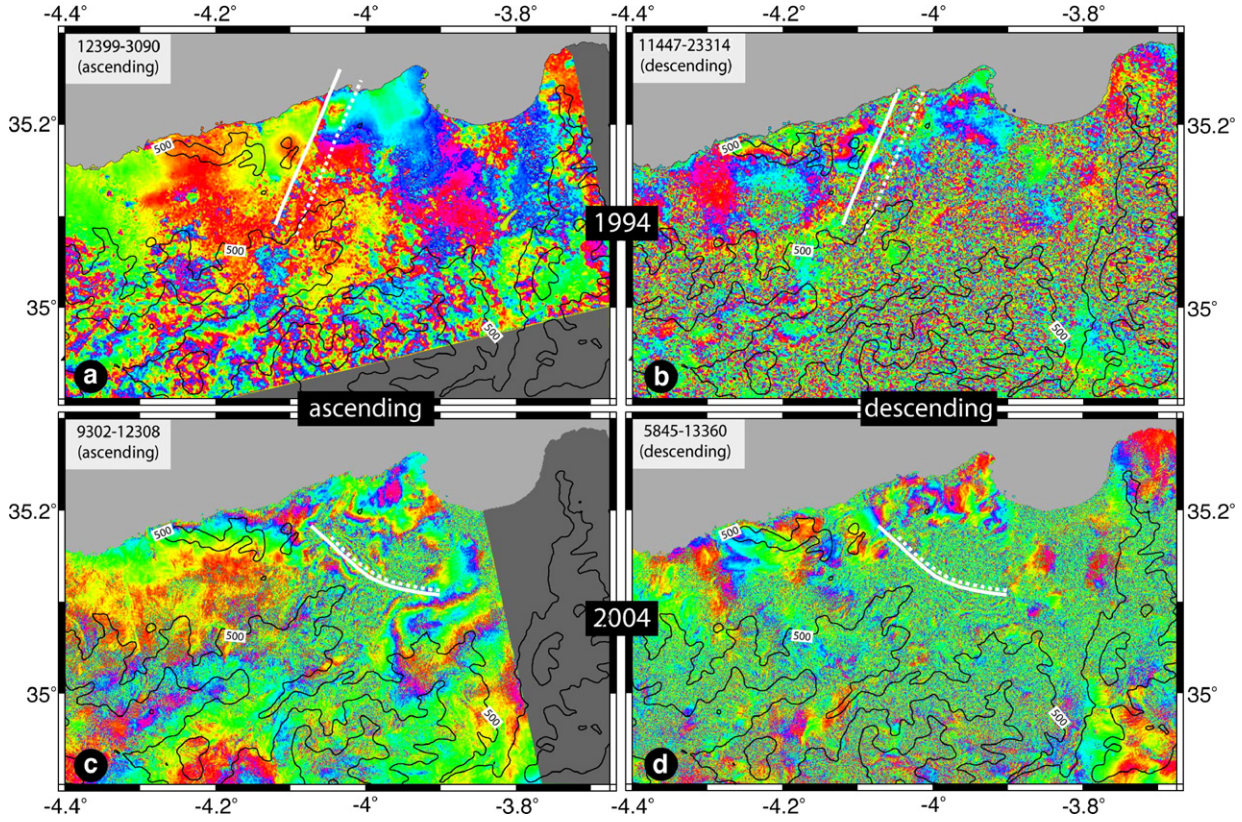

Fig. 8. Residual interferograms obtained after subtracting the synthetic interferograms (Fig. 7) from the observed data (Fig. 4). Black lines are topographic contours at every 500 m of elevation.

of the fringes that are readily visible could not be unwrapped without large errors due to the poor coherence to the south of the earthquake area (Fig. 4). The slip distribution on the triangular elements was then inverted with a negativity constraint on the strike–slip component (i.e. left-lateral for the 1994 fault and right-lateral for the 2004 fault). No sign constraints were imposed on the dip-slip component. To avoid unphysical oscillatory slip, the scale-dependent umbrella smoothing operator of Poly3-Dinv is applied to inverted slip distribution (with a factor of 0.3 for both earthquakes). Since we use digitized contours of fringes, the smoothing operator with a zero slip constraint on the fault edges, including the topmost patches, also prevents deducing high slip peaks where the inverted data are insufficient or absent (particularly at the fault termination). In addition, a uniform tilting in the data is searched to prevent any orbital errors from biasing the slip estimates.

In order to deduce the fault parameters of the 1994 earthquake we run series of inversions using both left and right-lateral faults with varying strike and dip even though all the previous studies [3,5,7] propose a left-lateral fault mechanism [Table 3]. The best fitting model (model 15 in Table 3) predicts a left-lateral fault rupture of about 16-km-long running between the town of El Hajbouke in the south to several kilometers offshore (~3 km) near Tafensa in the north. This is in good agreement with the distribution of aftershocks and, supports the inference of El Alami et al. [3] that the causative fault of the event is the Boussekkour fault (Fig. 3b). It strikes N23° E and dips towards the southeast at an angle of 77°, in good agreement with the Harvard CMT solution (Table 1). Since the modeled fault must not cross cut any visible fringes in the ascending or descending interferograms, the possible range for fault strike is quite narrow (±5°). The dip of the fault is established after a series of inversions with faults dipping from NW to SE (Fig. 5, Table 3). Our best slip model indicates that slips on the southern part of the fault have largely dip-slip component (i.e. normal faulting) with displacements reaching up to 0.8 m at 4 to 8 km of depth (Fig. 6). The dip-slip deduced explains the ground subsidence indicated by the presence of a common lobe between the ascending and descending interferograms, and is consistent with most of the focal mechanism solutions

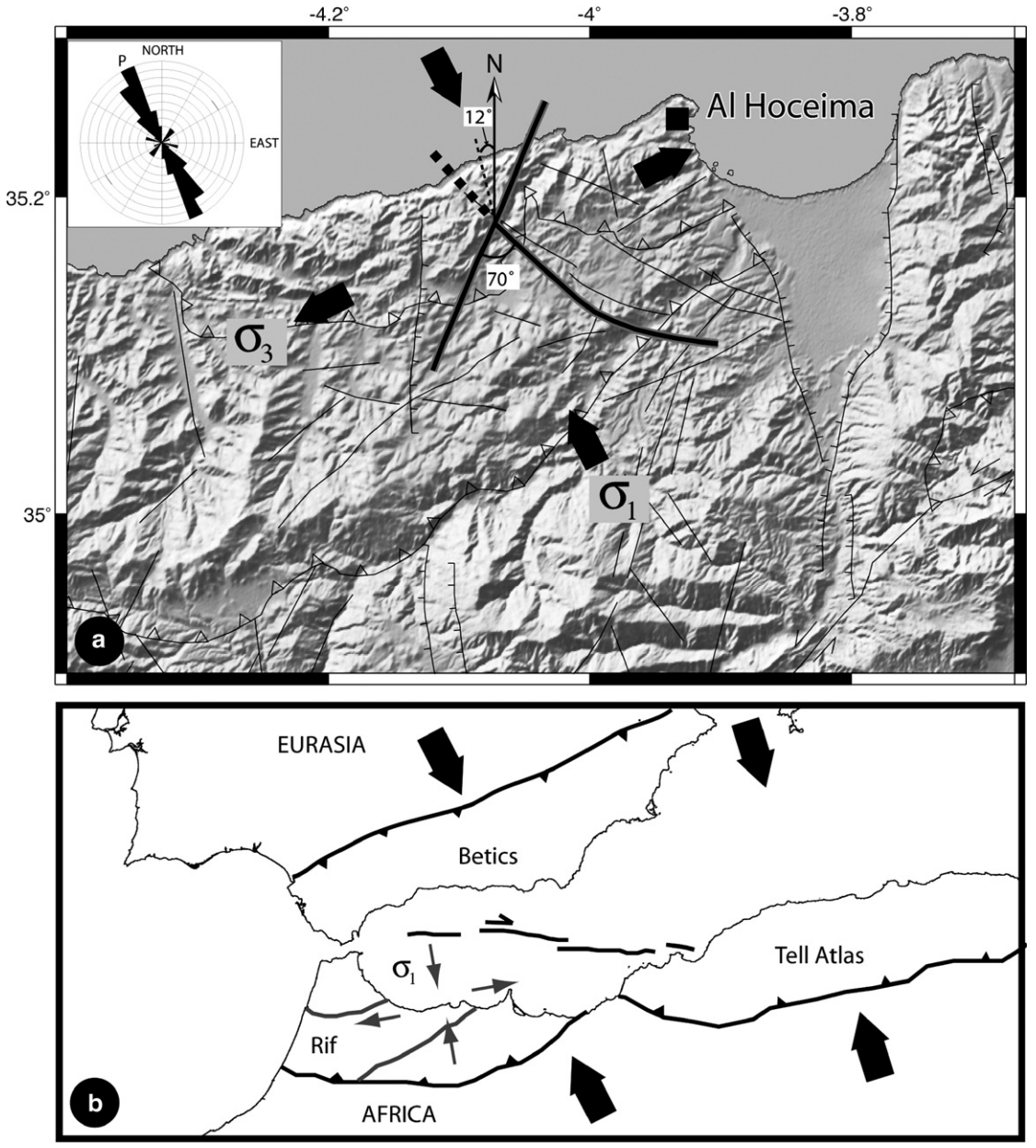

Fig. 9. (a) Stress field in the Al Hoceima region and block tectonic model associated with Africa–Eurasia (Iberia) plate boundary. Arrows show the direction of the maximum (σ_1) and minimum (σ_3) horizontal stresses based on seismic tensor inversion (from Medina [40]). Rose diagram shows *P*-axes orientation of 44 earthquakes that occurred in the region since 1968. (b) Block tectonic model with oblique plate convergence and transpression affecting the Rif, Betics and Tell Atlas Mountains. In this transpressive system, the N15° W shortening in the Rif bisects the angle between plate convergence vector and normal to the deforming zone [41].

deduced from seismology (Table 1). Towards the north, the displacement is mainly strike–slip with similar amplitudes (~0.9 m). It is worthwhile to note that the fault parameters of the earthquake are well constrained owing to the presence of ascending and descending interferograms. Because the surface deformation is imaged from two different positions (i.e. in ascending and descending view), the ambiguity whether the LOS range change is due to vertical or horizontal motion is largely solved [37].

We modeled the interferograms of the 2004 earthquake with a curved right-lateral strike–slip fault of about 19 km that dips 87–88° eastward with a strike changing from N85° W in the south, to N38° W in the

north (N45° W in average; Fig. 7). This fault geometry is the same as that of Cakir et al. [10] except that here, the fault length is shortened for a few kilometers from the northern edge to prevent the intersection with the modeled 1994 earthquake fault. The slip pattern deduced from the inversion shows two asperities separated by a low slip zone around the fault bend (Fig. 6). The asperity on the WNW–ESE trending part of the fault to the south releases approximately the 70% of the seismic moment with predominantly strike–slip displacements of up to 2.7 m at 7 km depth. Located slightly deeper (~9 km) on the fault near the 1994 rupture, the smaller asperity with a maximum slip of 1 m is now better revealed as compared to the previous model of Cakir et al. [10].

The inferred geodetic moments of 2.0×10^{18} Nm (Mw=6.1) and 6.6×10^{18} Nm (Mw 6.5) obtained from the modeling for 1994 and 2004 earthquake ruptures, respectively, are in good agreement with those obtained from seismological observations (Table 1). As shown in Fig. 7, the main features of the observed interferograms of the two earthquakes are successfully reproduced by the best slip models with RMS (root mean square) misfits well below an individual fringe (2.8 cm). The best fit between the modeled and observed interferograms is also revealed from the profiles and residual interferograms (i.e. models minus data) shown in Figs. 7e and 8. Some of the remaining fringes in the residual interferograms are most probably due to atmospheric artifacts and unmodeled fault complexity in the near field. For example, part of the phase west of the fault in the 1994 residual ascending interferogram (Fig. 8a) is most likely associated with homogenous atmospheric artifacts since there is a clear correlation between the phase and topographic elevation (Fig. 8a). Therefore, although small, this interferogram may also contain some homogenous atmospheric effects.

5. Discussion and conclusions

The analysis and modeling of InSAR data indicate that the May 26, 1994 (Mw=6.0) and February 24, 2004 (Mw=6.4) earthquake sequence occurred on conjugate strike–slip faults trending approximately N23° E and N45° W (Fig. 9a). The acute angle between the conjugate faults is thus roughly 70°, which is 5–10° greater than that expected from Coulomb friction in a homogeneous, unflawed, intact rock which, according to laboratory experiments [38], has a coefficient of friction between 0.6 and 0.85. This suggests that either the conjugate faults have low coefficient of friction or at least one of them is a pre-existing rupture plane reactivated under a relatively lower shear stress. Assuming an Anderson–Byerlee fault mechanics [39] which predicts that the maximum horizontal stress (σ_1) axis bisects the acute angle between the conjugate faults, the direction of σ_1 in the Al Hoceima and Rif region is ~N12° W, in good agreement with N15°–25° W direction determined from seismic tensor inversions [40] and the orientation of the *P*-axes of 44 earthquakes that occurred in the region between 1968 and 1994 (Fig. 9a). This may seem inconsistent to some extent with the NUVEL-1A plate motion [2] and GPS models [12] that predict a convergent direction of N40°–50° W. These models, however, do not integrate local block tectonics and possible local variations in the stress field along the plate boundary as they are based on large scale observations and sparse GPS measurements. Indeed, the discrepancy between the N40°–50° W convergence and the inferred N12° W horizontal stress σ_1 (Fig. 9a) can be in agreement if we consider the Rif region as an E–W trending deforming zone between the oblique convergence of the rigid Africa and Eurasia plates (Fig. 9b). In this transpressive system, the strike–slip partitioning induces a direction of shortening that bisects the angle between plate motion vector and normal to plate margin [41].

The occurrence of earthquakes on left- and right-lateral strike–slip faults supports the assumption that the Rif is subject to distributed strike–slip deformation [5]. Although the modeled fault of the 1994 event coincides with the Boussekkour fault (Fig. 3b), the 2004 earthquake took place on an unknown active fault. That the Nekor and Boussekkour faults are sub-parallel to each other implies that the Nekor fault is also optimally oriented in the present day stress field and thus may now be potentially accumulating elastic strain to be released in a future large earthquake. Therefore, the available maps of active faults capable of producing large earthquakes in the Rif should be reevaluated based on new field investigations using improved remote sensing techniques.

That the NW–SE to NE–SW trending faults including the 1994–2004 earthquake ruptures crosscut the thrust faults of the Rif (Fig. 3) reflects Quaternary strike–slip tectonics superimposed on Tertiary thrust-and-fold tectonics [17]. At present the strike–slip regime is probably on its early stages since geomorphological features associated with strike–slip faults are not well developed on the landscape. The focal solutions of earthquakes in the Rif Mountains (Fig. 1) indicate strike–slip mechanisms showing normal faulting component with N15° W σ_1 and N75° E σ_3 in agreement with a transpression tectonic model. Therefore, the conjugate system can be interpreted as fragmentation

with slip partitioning affecting the Rif tectonic block associated with a westward tectonic escape in the frame of the Africa–Eurasia (Iberia) collision tectonics (Fig. 9b;[16]).

Acknowledgements

InSAR data are copyrighted and obtained courtesy of the European Space Agency under the projects CAT1-2532 and AOTR-2436. We thank D. Pollard of Stanford University for Poly3D and Frantz Maerten for his support. We also would like to thank Dr Chuck Wicks and 2 anonymous reviewers for their insightful and constructive reviews that greatly improved the paper. This is part of the dissertation of the first author who is supported by EU-FP6 TR-Access Mobility Project. Most of the figures were plotted using GMT [42]. This is IPGS paper no 2006.04-UMR7516.

References

[1] L. Ait-Brahim, C. Nakhcha, B. Tadili, A. El Mrabet, N. Jabour, Structural analysis and interpretation of the surface deformations of the February 24th, 2004 Al Hoceima earthquake, EMSC-Newsl. 21 (2004) 10–12.

[2] C. DeMets, R.G. Gordon, D.F. Argus, S. Stein, Current plate motions, Geophys. J. Int. 101 (1990) 425–478.

[3] S.O. El Alami, B. Tadili, T.E. Cherkaoui, F. Medina, M. Ramdani, L. Ait-Brahim, M. Harnafi, The Al Hoceima earthquake of May 26, 1994 and its aftershocks: a seismotectonic study, Ann. Geophys. 41 (N 4) (1998) 519–537.

[4] N. Jabour, M. Kasmi, M. Menzhi, A. Birouk, L. Hni, Y. Hahou, Y. Timoulali, S. Badrane, The February 24th, 2004 Al Hoceima earthquake, Eur.-Mediterr. Seismol. Cent. Newsl. 21 (2004) 7–10.

[5] A. Calvert, F. Gomez, D. Seber, M. Barazangi, N. Jabour, A. Ibenbrahim, A. Demnati, An integrated geophysical investigation of recent seismicity in the Al-Hoceima Region of North Morocco, Bull. Seismol. Soc. Am. 87 (1997) 637–651.

[6] L. Dorbath, Y. Hahou, B. Delouis, C. Dorbath, J. Van Der Woerd, S. Badrane, M. Frogneux, H. Haessler, E. Jacques, M. Menzhi, P. Tapponnier, Études sismologiques sur le séisme D'al Hoceima: Localisation, et mécanisme du choc principal et des répliques, contraintes et structure de la zone epicentrale, Colloque Intenational Seisme d'Al Hoceima: bilan et perspectives. Al Hoceima, Morocco, February 24–26 2005.

[7] M. Bezzeghoud, E. Buforn, Source parameters of the 1992 Melilla (Spain, Mw 4.8), 1994 Alhoceima (Morocco, Mw 5.8) and 1994 Mascara (Algeria, Mw 5.7) earthquakes and seismotectonic implications, Bull. Seismol. Soc. Am. 89 (1999) 359–372.

[8] E. Buforn, M. Bezzeghoud, C. del Fresno, J.F. Borges, R. Madariaga, A. Udías, Study of the fracture process of Al Hoceima earthquake (24/02/2004, Mw=6.2) from regional and teleseismic data, Geophys. Res. Abstr. 7 (2005) 05301 SRef-ID: 1607-7962/gra/EGU05-A-05301.

[9] D. Stich, F. de Lis Mancilla, D. Baumont, J. Morales, Source analysis of the Mw6.3, 2004, Al Hoceima earthquake (Morocco) using regional apparent source time functions, J. Geophys. Res. 110 (2005) B06306, doi:10.1029/2004JB003366.

[10] Z. Cakir, M. Meghraoui, A.M. Akoglu, N. Jabour, S. Belabbes, L. Ait-Brahim, Surface deformation associated with the Mw 6.4, February 24, 2004 Al Hoceima (Morocco) earthquake deduced from InSAR: implications for the active tectonics along North Africa, Bull. Seismol. Soc. Am. 96 (2006) 1–10, doi:10.1785/0120050108.

[11] M.A. Comninou, J. Dunders, The angular dislocation in a half space, J. Elast. 5 (1975) 203–216.

[12] J.-M. Nocquet, E. Calais, Geodetic measurements of crustal deformation in the western Mediterranean and Europe, Pure Appl. Geophys. 161 (2004) 661–681, doi:10.1007/s00024-003-2468 (0033–4553/04/030661 – 21).

[13] S. McClusky, R. Reilinger, S. Mahmoud, D. Ben Sari, A. Tealeb, GPS constraints on Africa (Nubia) and Arabia plate motions, Geophys. J. Int. 155 (2003) 126–138, doi:10.1046/j.1365-246X.2003.02023.

[14] E. Buforn, M. Bezzeghoud, A. Udias, C. Pro, Seismic sources on the Iberia–African plate boundary and their tectonic implications, Pure Appl. Geophys. 161 (2004) 623–646.

[15] N. Grimison, W. Cheng, The Azores–Gibraltar plate boundary: focal mechanisms, depths of earthquakes and their tectonic implications, J. Geophys. Res. 91 (1986) 2029–2047.

[16] J.L. Morel, M. Meghraoui, The Goringe–Alboran–Tell tectonic zone, a transpression system along the Africa–Eurasia plate boundary, Geology 24 (1996) 755–758.

[17] M. Meghraoui, J.L. Morel, J. Andrieux, M. Dahmani, Tectonique plio-quaternaire de la chaîne tello-rifaine et de la mer d'Alboran; une zone complexe de convergence continent, Bull. Soc. Geol. Fr. 167 (1) (1996) 141–157.

[18] M. Ramdani, B. Tadili, T. El Mrabet, The present state of knowledge on historical seismicity of Morocco, in: G. Payo, C. Radu, D. Postpischil (Eds.), Proceedings of the Symposium on Calibration of Historical Earthquakes in Europe and Recent Developments in Intensity Interpretation, European Seismological Commission, Instituto Geográfico Nacional, Madrid, 1989, pp. 257–279.

[19] D. Frizon de Lamotte, Un exemple de collage synmetamorphe: la deformation miocene des Temsamane (Rif externe, Maroc), Bull Soc. Geol. Fr. 3 (1987) 337–344.

[20] D. Hatzfeld, V. Caillot, T.-E. Cherkaoui, H. Jebli, F. Medina, Microearthquake seismicity and fault plane solutions around the Nekor strike-fault, Morocco, Earth Planet. Sci. Lett. 120 (1993) 31–41.

[21] D. Massonnet, M. Rossi, C. Carmona, F. Adragna, G. Peltzer, K. Feigl, T. Rabaute, The displacement field of the Landers earthquake mapped by radar interferometry, Nature 364 (1993) 138–142.

[22] R. Bürgmann, P. Rosen, E. Fielding, Synthetic aperture radar interferometry to measure Earth′s surface topography and its deformation, Ann. Rev. Earth Planet. Sci. 28 (2000) 169–209.

[23] G. Peltzer, P. Rosen, F. Rogez, K. Hudnut, Postseismic rebound in fault step-overs caused by pore fluid flow, Science 273 (1996) 1202–1204.

[24] R. Bürgmann, D. Schmidt, R.M. Nadeau, M. d'Alessio, E. Fielding, D. Manaker, T.V. McEvilly, M.H. Murray, Earthquake potential along the northern Hayward fault, California, Science 289 (2000) 1178–1181.

[25] Z. Cakir, A.M. Akoglu, S. Belabbes, S. Ergintav, M. Meghraoui, Creeping along the North Anatolian Fault at Ismetpasa (Western Turkey): rate and extent from InSAR, Earth Planet. Sci. Lett. 238 (2005) 225–234.

[26] P.A. Rosen, S. Hensley, G. Peltzer, M. Simons, Updated repeat orbit interferometry package released, Eos, Trans. - Am. Geophys. Union 85 (2004) 35.

[27] B. Kampes, R. Hanssen, Z. Perski, Radar interferometry with public domain tools, Proceedings of FRINGE 2003, December 1–5, Frascati, Italy, 2003.
[28] R. Scharoo, P. Visser, Precise orbit determination and gravity field improvement for the ERS satellites, J. Geophys. Res. 103 (1998) 8113–8127.
[29] T. Farr, M. Kobrick, Shuttle Radar Topography Mission produces a wealth of data, Eos, Trans. - Am. Geophys. Union 81 (2000) 583–585.
[30] R. Goldstein, C. Werner, Radar interferogram filtering for geophysical applications, Geophys. Res. Lett. 25 (1998) 4035–4038.
[31] F. Amelung, J.W. Bell, Interferometric synthetic aperture radar observations of the 1994 Double Spring Flat, Nevada earthquake (M5.9): mainshock accompanied by triggered slip on a conjugate fault, J. Geophys. Res. 108 (B9) (2003) (ETG 10-1-10-11).
[32] M. Talebian, J. Biggs, M. Bolourchi, A. Copley, A. Ghassemi, M. Ghorashi, J. Hollingsworth, J.A. Jackson, E. Nissen, B. Oveisi, B.E. Parsons, K. Priestley, The Dahiuyeh (Zarand) earthquake of 2005 February 22 in central Iran: reactivation of an intramountain reverse fault, Geophys. J. Int. 164 (2006) 137–148.
[33] G. Funning, B.E. Parsons, T.J. Wright, J.A. Jackson, E.J. Fielding, Surface displacements and source parameters of the 2003 Bam (Iran) earthquake from Envisat advanced synthetic aperature radar imagery, J. Geophys. Res. 110 (2005) B09406, doi:10.1029/2004JB003338.
[34] F. Maerten, P.G. Resor, D.D. Pollard, L. Maerten, Inverting for slip on three-dimensional fault surfaces using angular dislocations, Bull Seismol. Soc. Am. 95 (2005) 1654–1665.
[35] A.L. Thomas, Poly3D: a three-dimensional, polygonal element, displacement discontinuity boundary element computer program with applications to fractures, faults, and cavities in the earth's crust. M.S. Thesis, Stanford University, Stanford, California, 221p. 1993.
[36] P.G. Resor, D.D. Pollard, T.J. Wright, G.C. Beroza, Integrating high-precision aftershock locations and geodetic observations to model coseismic deformation associated with the 1995 Kozani–Grevena earthquake, Greece, J. Geophys. Res. 110 (2005) B09402, doi:10.1029/2004JB003263.
[37] T.J. Wright, B.E. Parsons, Z. Lu, Toward mapping surface deformation in three dimensions using InSAR, Geophys. Res. Lett. 31 (2004) L01607, doi:10.1029/2003GL018827.
[38] J. Byerlee, Friction of rocks, Pure Appl. Geophys. 116 (1978) 615–626.
[39] E.M. Anderson, The Dynamics of Faulting and Dyke Formation with Applications to Britain, Oliver and Boyd, Edinburgh, 1951.
[40] F. Medina, Present-day state of stress in northern Morocco from focal mechanism analysis, J. Struct. Geol. 17 (7) (1995) 1035–1046.
[41] C. Teyssier, B. Tikoff, M. Markley, Oblique plate motion and continental tectonics, Geology 23 (1995) 447–450.
[42] P. Wessel, W.H.F. Smith, Free software helps map and display data, Eos, Trans. - Am. Geophys. Union 72 (1991) 445–446.
[43] L. Ait-Brahim, B. Tadili, C. Nakhcha, I. Mouayn, M. Ramdani, M. Limouri, A. ElQadi, F. Sossey Alaoui, M. Benhalima, Modeling in the Eastern Rif (Northern Morocco) using active faults and seismicity for the strong motion, Pure Appl. Geophys. 161 (2004) 10811091, doi:10.1007/s00024-003-2487-9 (0033–4553/04/061081–11).